Casimir forces from conductive silicon carbide surfaces

M. Sedighi,[1] V. B. Svetovoy,[2,3] W. H. Broer,[1] and G. Palasantzas[1]

[1]*Zernike Institute for Advanced Materials, University of Groningen, Nijenborgh 4, 9747 AG Groningen, The Netherlands*

[2]*MESA+ Institute for Nanotechnology, University of Twente, P.O. Box 217, 7500 AE Enschede, The Netherlands*

[3]*Institute of Physics and Technology, Yaroslavl Branch, Russian Academy of Sciences, 150007, Yaroslavl, Russia*

(Received 26 February 2014; revised manuscript received 1 May 2014; published 27 May 2014)

Samples of conductive silicon carbide (SiC), which is a promising material due to its excellent properties for devices operating in severe environments, were characterized with the atomic force microscope for roughness, and the optical properties were measured with ellipsometry in a wide range of frequencies. The samples show significant far-infrared absorption due to concentration of charge carriers and a sharp surface phonon-polariton peak. The Casimir interaction of SiC with different materials is calculated and discussed. As a result of the infrared structure and beyond to low frequencies, the Casimir force for SiC-SiC and SiC-Au approaches very slowly the limit of ideal metals, while it saturates significantly below this limit if interaction with insulators takes place (SiC-SiO_2). At short separations (<10 nm) analysis of the van der Waals force yielded Hamaker constants for SiC-SiC interactions lower but comparable to those of metals, which is of significance to adhesion and surface assembly processes. Finally, bifurcation analysis of microelectromechanical system actuation indicated that SiC can enhance the regime of stable equilibria against stiction.

DOI: 10.1103/PhysRevB.89.195440 PACS number(s): 64.70.Nd, 85.85.+j, 12.20.Fv

I. INTRODUCTION

Nowadays fluctuation induced electromagnetic (EM) forces between neutral bodies attract more and more interest in device physics toward technology applications [1]. These forces between two objects arise due to perturbation of quantum fluctuations of the EM field [1–12], as was predicted by Casimir in 1948 [2] assuming two perfectly conducting parallel plates. Soon after, Lifshitz and co-workers in the 1950s [3] considered the general case of real dielectric plates by exploiting the fluctuation-dissipation theorem, which relates the dissipative properties of the plates (optical absorption by many microscopic dipoles) and the resulting EM fluctuations. The theory describes correctly the attractive interaction due to quantum fluctuations for all separations covering both the Casimir (long-range) and van der Waals (vdW) (short-range) regimes [1,3,4]. In any case, the dependence of the Casimir force on materials is an important topic since in principle one can tailor the force by suitable choice of materials [5–12].

Up to now there is a significant variety of materials used [5–12] for calculations and measurements of the Casimir force. It has been confirmed that metals are the materials (e.g., Au is the one studied the most) that give the maximum Casimir force due to high absorption of conduction electrons in the low-frequency ranges (far-infrared). However, metals are not always suitable for device applications if attributes such as high durability combined with high stiffness and low thermal expansion are necessary. On the other hand, a material that offers these properties is SiC, and it is currently utilized for precise instrumentation frames and mirrors, as well as there is a possibility to be used in macro- and nanoassembly technologies via direct (optical) bonding concepts [13]. Moreover, in microelectromechanical systems (MEMS) applications for industry, automotive, and space applications [14,15], MEMS sensors are required to operate in harsh environments, which can be a challenge for Si sensing devices. Instead SiC is considered a substitute for Si due to its excellent properties.

SiC is a material that exhibits strong polytypism, where all polytypes have identical planar arrangement, while the difference lies in the stacking of the planes. Disorder in the stacking periodicity of similar planes results in different types of polytypes (≥ 250). The relatively low residual stress level in the layers, the high stiffness, and excellent etch-stop properties allow the fabrication of free-standing SiC microstructures using standard Si bulk micromachining techniques [14,15]. In addition, since SiC exhibits high hardness, chemical inertness, and ability to survive operation at high temperatures and harsh environments, it is well suited to be used as a protective coating of micromachined parts. Therefore we will characterize here the properties of vdW and Casimir forces from conductive SiC surfaces, and the corresponding implications in simple MEMS actuation. In order to minimize charging and electrostatic effects in device applications we have chosen to study conductive SiC samples.

II. PROPERTIES OF CONDUCTIVE SILICON CARBIDE

Nitrogen (N) doped SiC samples of SiC [thickness 400 μm and chemical-mechanical polished (CMP)] were obtained from University Wafers (http://www.universitywafer.com/). The optical properties of the SiC samples were commercially characterized in J. A. Woollam Co., Inc. (http://www.jawoollam.com) with ellipsometry using the VUV-VASE (0.5–9.34 eV) and IR-VASE (0.03–0.5 eV) ellipsometers at three incident angles (with respect to the sample surface) $\varphi = 55°, 65°, 75°$ (see Supplemental Material, Eq. (A1) [16]). Furthermore, the analysis was performed as in [11] to obtain the real and imaginary parts of the frequency-dependent dielectric function $\varepsilon(\omega)$.

Atomic force microscopy (AFM) analysis indicated an almost atomically flat surface with a root-mean-square (rms) surface roughness ~ 0.12 nm (see Supplemental Material, Fig. B1 [16]) making roughness contributions to optical data negligible. Moreover, Casimir force measurement on these

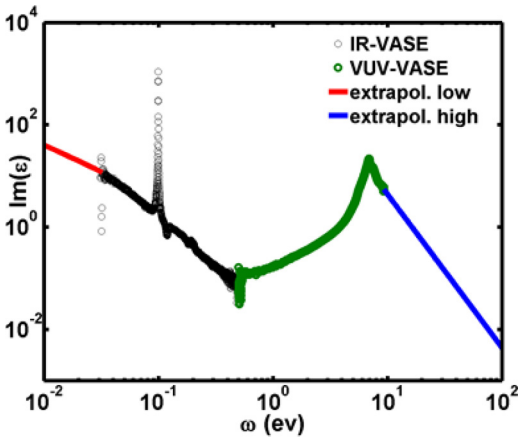

FIG. 1. (Color online) Here we show the imaginary part $\varepsilon''(\omega)$, enlarged by the extrapolated regions, combining the ellipsometric data (circles) from IR-VASE (for $0.03<\omega<0.5$ eV) and all data from the VUV-VASE. For the experimentally inaccessible frequencies $\varepsilon''(\omega)$ was extrapolated via Eq. (3) (solid lines).

samples using smooth spheres (e.g., boron silicate [17]) would allow one to reach separations limiting the roughness upon contact down to ∼5 nm [18]. In any case, it remains important to know beforehand what force levels are to be expected from SiC surfaces over separation ranges less than 300 nm that are relevant for micro- and nanodevice applications.

Because the data from the IR-VASE (Fig. 1 and see Supplemental Material, Fig. C1 [16]) are noisy at both ends of the measurement range, while the data from the VUV-VASE are less noisy, we use data from the VUV-VASE where they overlap with the IR-VASE data. Thus, we will limit the use of the IR-VASE data in the frequency range $0.03<\omega<0.5$ eV (see Supplemental Material, Fig. C1 [16]). The data for $0.03<\omega<0.11$ eV can be described by the Drude model, corresponding to charge carriers due to doping, and the surface phonon-polariton at $\omega = 0.099$eV, which yields the peak in Fig. 1. For this range the data can be fitted by

$$\varepsilon(\omega) = \varepsilon_\infty - \frac{\omega_p^2}{\omega(\omega + i\omega_\tau)} + \frac{\varepsilon_\infty\left(\omega_L^2 - \omega_T^2\right)}{\left(\omega_T^2 - \omega^2 - i\Gamma\omega\right)}, \qquad (1)$$

where ω_T and ω_L are transverse and longitudinal optical phonon frequencies and Γ is the width of the phonon-polariton peak. The fits (see Supplemental Material, Fig. C2 [16]) yield the parameters $\varepsilon_\infty = 6.15$, $\omega_p = 0.173$ eV, $\omega_\tau = 0.074$ eV, $\omega_L = 0.122$ eV,, $\omega_T = 0.099$ eV,, and $\Gamma = 2.88 \times 10^{-4}$ eV. For very low frequencies, $\omega \ll \omega_\tau$, the Drude term diverges with the frequency as $\varepsilon(\omega) \cong \varepsilon_\infty + i[(\omega_p^2/\omega_\tau)/\omega]$ where the ratio ω_p^2/ω_τ yields the sample conductivity $\sigma = (\omega_p^2/\omega_\tau)/4\pi$. Note that for Ohmic materials the Maxwell equations yield in the quasistatic limit $\omega \to 0$: $\varepsilon''(\omega) \cong 4\pi\sigma/\omega$. For SiC we have $\omega_p^2/\omega_\tau|_{\rm SiC} = 0.4$ eV, while for comparison to metals, i.e., Au, $\omega_p^2/\omega_\tau|_{\rm Au} \approx 1600$ eV [11]. Finally, the parameters of the phonon-polariton peak compare well with literature values [19]: $\varepsilon_\infty = 6.7$, $\omega_L = 0.12$ eV, $\omega_T = 0.098$ eV, and $\Gamma \approx 5.88 \times 10^{-4}$ eV.

For the force calculations via the Lifshitz theory we need the function $\varepsilon(i\zeta)$

$$\varepsilon(i\zeta) = 1 + \frac{2}{\pi}\int_0^\infty \frac{\omega\varepsilon''(\omega)}{\omega^2 + \zeta^2}d\omega. \qquad (2)$$

To find the force we use the procedure that relies maximally on the experimental information about the dielectric function [11]. Within the interval $\omega_1 < \omega < \omega_2$, where $\omega_1 = 0.03$ eV and $\omega_2 = 9.34$ eV, the experimental data for $\varepsilon(\omega)$ are used. At low and high frequencies, $\omega < \omega_1$ and $\omega > \omega_2$, respectively, where no data are experimentally available, $\varepsilon''(\omega)$ is extrapolated via the equations

$$\omega < \omega_1 : \varepsilon''(\omega) = \frac{\omega_p^2\omega_\tau}{\omega\left(\omega^2 + \omega_\tau^2\right)} \quad \text{and} \quad \omega > \omega_2 : \varepsilon''(\omega) = \frac{A}{\omega^3}. \qquad (3)$$

The constant A in Eq. (3) is determined by continuity of $\varepsilon''(\omega)$ at $\omega = \omega_2$. The contributions of these frequency ranges to $\varepsilon(i\zeta)$ are given by the analytic forms

$$\begin{aligned}\Delta_H\varepsilon(i\zeta) &= \frac{2}{\pi}\int_{\omega_2}^\infty \frac{\omega\varepsilon''(\omega)}{\omega^2 + \zeta^2}d\omega \\ &= \frac{2\omega_2^3\varepsilon''(\omega_2)}{\pi\zeta^2}\left[\frac{1}{\omega_2} - \frac{\frac{\pi}{2} - \arctan(\omega_2/\zeta)}{\zeta}\right], \\ \Delta_L\varepsilon(i\zeta) &= \frac{2}{\pi}\int_0^{\omega_1} \frac{\omega\varepsilon''(\omega)}{\omega^2 + \zeta^2}d\omega \\ &= \frac{2\omega_p^2\omega_\tau}{\pi\left(\zeta^2 - \omega_\tau^2\right)}\left[\frac{\arctan(\omega_1/\omega_\tau)}{\omega_\tau} - \frac{\arctan(\omega_1/\zeta)}{\zeta}\right].\end{aligned} \qquad (4)$$

Therefore the dielectric function at imaginary frequencies obtains the form

$$\varepsilon(i\zeta) = 1 + \frac{2}{\pi}\int_{\omega_1}^{\omega_2} \frac{\omega\varepsilon''_{\rm exp}(\omega)}{\omega^2 + \zeta^2}d\omega + \Delta_L\varepsilon(i\zeta) + \Delta_H\varepsilon(i\zeta). \qquad (5)$$

Figure 2 shows the contributions of $\Delta_{L,H}\varepsilon(i\zeta)$ on $\varepsilon(i\zeta)$, from where it is evident the significance of the low-frequency contribution $\Delta_L\varepsilon(i\zeta)$ at large separations z or small $\zeta \sim c/z$. The contribution of high frequencies can be important at small distances.

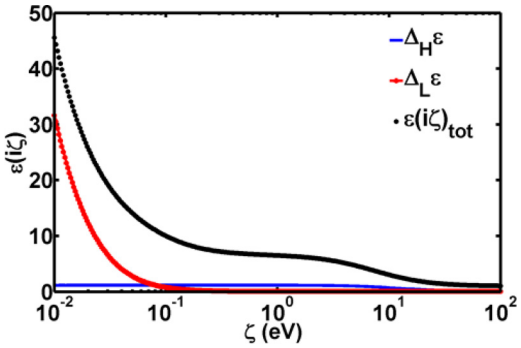

FIG. 2. (Color online) The dielectric function of SiC at imaginary frequencies (open circles). The contribution of low and high frequencies are given by the red and blue curves, respectively.

III. FORCE CALCULATIONS: PLANE-PLANE GEOMETRY

From the plasma frequency ω_p, we can estimate the concentration of conduction carriers $N_e = m^*\omega_p^2/4\pi e^2$ in SiC, if the effective carrier mass m^* is close to the mass of the free electrons. Thus we obtain $N_e \cong 2.2 \times 10^{19}\text{cm}^{-3}$. This is a sufficiently high concentration of charge carriers so that one can neglect the effects of poor conductivity resulting in nonlocal response of the material. Indeed, the Debye screening length $l_D = \sqrt{\varepsilon_{\text{SiC}} K_B T/4\pi N_e e^2}$ (with T the system temperature and K_B the Boltzmann constant) has the value for our system $l_D \approx 1\text{nm}$. Hence for separations between interacting bodies $z > l_D$ we can neglect charge distributions in the material. Moreover, thermal effects at the separations $l_D < z \lesssim 300\text{nm}$ can be neglected. In this case we calculate the Casimir force at zero temperature $T = 0$, for which one of the convenient representations is

$$F(z) = \frac{\hbar c}{32\pi^2 z^4} \sum_{\nu} \int_0^1 dt \int_0^\infty dx x^3 \frac{r_1^\nu r_2^\nu e^{-x}}{1 - r_1^\nu r_2^\nu e^{-x}}. \quad (6)$$

Here the integration variables are defined as $x = 2k_0 z$, $tx = \zeta/\zeta_{ch}$, and $\zeta_{ch} = c/2z$. The index $\nu = s$(TE mode) or p(TM mode) denotes the two polarizations, and $r_{1,2}^\nu$ are the reflection coefficients for body 1 or 2. The wave numbers perpendicular to the plates in vacuum are $k_0 = \sqrt{(\zeta^2/c^2) + q^2}$, and in the ith material $k_i = \sqrt{\varepsilon_i(i\zeta)(\zeta^2/c^2) + q^2}$ where q is the wave number along the plates. Finally, the reflection coefficients (for nonmagnetic materials) are defined as

$$r_i^s = \frac{1 - \sqrt{1 + t^2[\varepsilon_i(i\zeta) - 1]}}{1 + \sqrt{1 + t^2[\varepsilon_i(i\zeta) - 1]}},$$
$$r_i^p = \frac{\varepsilon_i - \sqrt{1 + t^2[\varepsilon_i(i\zeta) - 1]}}{\varepsilon_i + \sqrt{1 + t^2[\varepsilon_i(i\zeta) - 1]}}. \quad (7)$$

First we have calculated the force between similar plates in the SiC-SiC surfaces. The function $\varepsilon(i\zeta)$ was calculated from the experimental data as described above in the interval $0.01 < \zeta < 100$ eV and outside of this interval we can continue it as $\varepsilon(i\zeta) \cong 9.34 + (a/\zeta)$ for small $\zeta (< 0.01$ eV), and as $\varepsilon(i\zeta) \cong 1 + (A/\zeta^2)$ for large $\zeta (> 100$ eV) for completeness-only purposes. In contrast with the extrapolation at real frequencies the extrapolations at large and small ζ do not play a significant role. The force results are presented in Fig. 3(a), where the force is normalized by the Casimir force $F_C(z)$ for ideal metals via the reduction factor

$$\eta(z) = \frac{F(z)}{F_C(z)}, \quad F_C(z) = \frac{\pi^2 \hbar c}{240} \frac{1}{z^4}. \quad (8)$$

The Casimir force (reduction factor) is shown in Fig. 3 by open circles, in the same way as for $\varepsilon(i\zeta)$ in Fig. 2, where the effect of omitting $\Delta_L\varepsilon(i\zeta)$ and $\Delta_H\varepsilon(i\zeta)$ is also shown. The result is given in a wide range of separation distances to demonstrate the very slow transition to the case of ideal metals ($\eta \to 1$).

The deviation of the force curve, which corresponds to the dielectric function with $\varepsilon''(\omega > 9.34\text{ eV}) = 0$ (no high), at small distances means that the contribution of high frequencies $\omega > 9.34$ eV [and thus $\Delta_H\varepsilon(i\zeta)$], is important at small separations. For larger separation distances the reduction factor is not saturated as fast as for the example of two Au-Au plates [11]. This is because the dielectric response function for SiC has structure at low frequencies and the Drude contribution is significantly weaker with respect to that of Au (and in general for metals) [11]. As a result the reduction factor $\eta(z)$ approaches 1 (ideal limit) only for very large distances $z > 1$ mm, where also the Casimir force is already extremely small. On the other hand the force curve, which corresponds to the dielectric function without low-frequency contribution or $\varepsilon''(\omega < 0.03\text{ eV}) = 0$ (no low), shows that the contribution of low frequencies [and thus $\Delta_L\varepsilon(i\zeta)$] becomes important at large separations $z > 1$ μm.

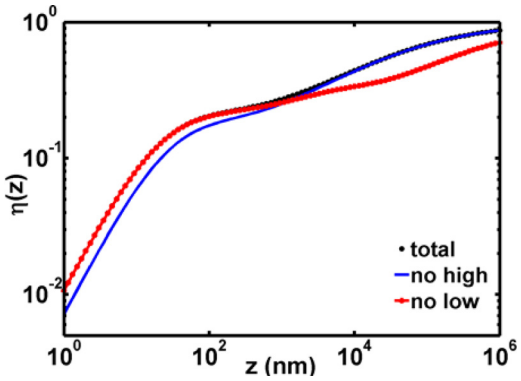

FIG. 3. (Color online) Casimir reduction factor $\eta(z)$ for SiC-SiC parallel plates as a function of separation. The effects of the omission of high- and low-frequency contribution are indicated.

The deviations of the force curves in Fig. 3 yield the maximum error that can occur due to extrapolation to low and high frequencies of the imaginary part $\varepsilon''(\omega)$ of the dielectric function. The realistic errors are much smaller because the main effect is taken into account by the extrapolations. The effect of omission of low frequencies can be neglected in the practical range of separation distances 3 nm $< z <$ 300 nm, while the maximal effect of high frequencies increases from 15% at 100 nm up to 30% at 1 nm as can be seen

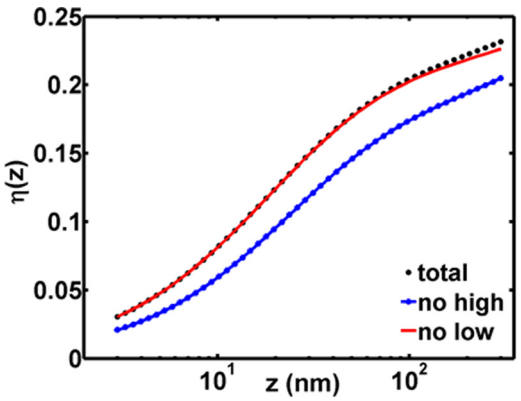

FIG. 4. (Color online) Force curves as in Fig. 3 but for a more detailed comparison with possible experiments for separations 3 nm $< z <$ 300 nm. Here we can see clearly the error by omission of the experimentally not-accessible high- and low-frequency regimes.

in Fig. 4. The latter shows a more detailed comparison for possible experiments at separations 3 nm $< z <$ 300 nm.

Finally, if we look at small distances, $z<10$ nm, then the force is the well-known van der Waals (vdW) force. If we consider the expression for the vdW force between plates,

$$F_{\rm vdW}(z) = \frac{A_H}{6\pi z^3}, \tag{9}$$

with A_H the Hamaker constant, then our calculations give for the SiC-SiC system the value $A_H = 16.5 \times 10^{-20}$J. This is lower than that of the Au-Au system where the experimentally obtained values were $A_H = (28 \pm 0.02)\times 10^{-20}$ J [20], while theory yielded $A_H \approx 40\times 10^{-20}$ J [21]. Therefore the Hamaker constants for SiC-SiC interactions are comparable to those of metallic systems, which can be of significance for high-adhesion-assembly processes.

IV. THE FORCE BETWEEN SiC PLATE AND A SPHERE

Because the Casimir force is usually measured using the sphere-plate geometry to avoid parallelism problems [8–12], which is a cumbersome issue at nanoscales, we will also examine details of force for this geometry. In this case the Casimir force is given by

$$F^{ps}(z) = \frac{\hbar c R}{16\pi z^3}\sum_{\nu}\int_0^1 dt\int_0^\infty dx\, x^2 \ln\left(1 - r_1^{\nu} r_2^{\nu} e^{-x}\right), \tag{10}$$

where R is the sphere radius so that $R \gg z$ [12]. Therefore our calculations in this geometry were restricted to separations $z \leq 1$ μm for sphere radius $R = 20$ μm. We also introduce here the reduction factor $\eta^{ps}(z)$, with respect to a sphere and plate made of ideal metal,

$$\eta^{ps}(z) = \frac{F^{ps}(z)}{F_C^{ps}(z)}, \quad F_C^{ps}(z) = \frac{\pi^3 R\hbar c}{360}\frac{1}{z^3}. \tag{11}$$

The behavior of $\eta^{ps}(z)$ versus separation is shown in Fig. 5 for a SiC plate and an Au-coated sphere (conductor) as well as a glass (insulator) sphere. The dielectric function of Au is from sample 3 in [11]. For SiC the total dielectric function was used for the force calculations. Similarly when we calculate the force between a SiC plate and a glass sphere, it is assumed that no residual charges are present on the sphere. The dielectric function of glass was taken from the Palik data for quartz [22]. Although real glass can behave slightly differently optically, the difference in the force is not large.

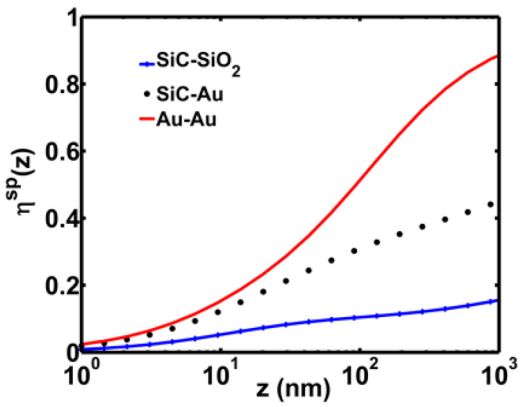

FIG. 5. (Color online) Casimir reduction factor $\eta^{ps}(z)$ for different pairs of materials (SiC-Au, SiC-SiO_2, and Au-Au). Note that for the Au-Au the redaction factor at 100 nm is nearly two times larger than that for SiC-Au, but for a distance of 50 nm the difference is significantly reduced.

From Fig. 5 it is interesting to note that for both SiC-Au and SiC-SiO_2 the reduction factor is far from saturation for the largest distances $z \leqslant 1$ μm. This is the result of nontrivial optical structure of both SiC and SiO_2. Only at very large distances does SiC start to look like an ideal metal and the reduction factor approaches unity, $\eta^{sp}(z) \to 1$, for the SiC-Au interaction only. Glass, however, is not conductive and for this reason the reduction factor $\eta^{sp}(z)$ is saturated at a smaller value [$\eta^{sp}(z) < 1$], which is defined by the static permittivity of SiO_2 (for the detailed behavior of the curves for SiC-Au and SiC-SiO_2 in the practical distance range 3–300 nm see also Supplemental Material, Fig. D1 [16]).

V. MATERIALS INFLUENCE ON MEMS ACTUATION

In order to better understand the influence of the Casimir force from SiC surfaces on MEMS actuation, we consider [Fig. 6(a)] a moving sphere and a fixed plate coated both with a thick (optical thickness $\geq$100 nm) coating of SiC or Au for comparison purposes. The Casimir force in the sphere-plate geometry (which is widely used in force measurements by AFM and MEMS) [8–12] is given by Eq. (10). The elastic restoring force $F_K(z) = -K(L_0 - z)$ of the spring with stiffness K counterbalances the attractive Casimir force $F_C(z)$. The equation of motion, assuming an initial impulse to trigger continuous actuation from an initial separation L_0 where the spring is not stretched ($K \gg |\partial F_C/\partial z|_{z=L_0}$), has the form [23,24]

$$M\frac{d^2z}{dt^2} + \left(\frac{M\omega}{Q}\right)\left(\frac{dz}{dt}\right) = -K(L_0 - z) + F^{ps}(z). \tag{12}$$

M is the mass of the sphere, and the dissipative term $(M\omega/Q)(dz/dt)$ represents energy losses due to intrinsic dissipation of the actuating system associated with a quality factor Q for motion in vacuum. Here we consider high-quality factor system $Q>10^4$ [25] so that we can neglect dissipation effects, and actuators with resonance frequency $\omega = 300$ kHz (typical for AFM cantilevers and other MEMS) [26].

To obtain the equilibrium points of motion from Eq. (13) we define the bifurcation parameter $\lambda = F_{\rm SiC}^{ps}(L_0)/KL_0$ [23,24], which is the ratio of the minimal Casimir force $F_{\rm SiC}^{ps}(L_0)$ (for SiC) and the maximum elastic restoring force KL_0, representing the relative importance of one force competing with the other. The locus of equilibrium points z^* is obtained from Eq. (12) if we set the total force $F_T = -K(L_0 - z^*) + F^{ps}(z^*) = 0$ [23,24]. Solution yields for the parameter bifurcation parameter λ,

$$\lambda = \left[F_{\rm SiC}^{ps}(L_0)/F^{ps}(z^*)\right](1 - z^*/L_0). \tag{13}$$

The critical equilibrium points where stiction occurs are characterized also by the condition $dF_T/dz^* = K + dF^{ps}/dz^* =$

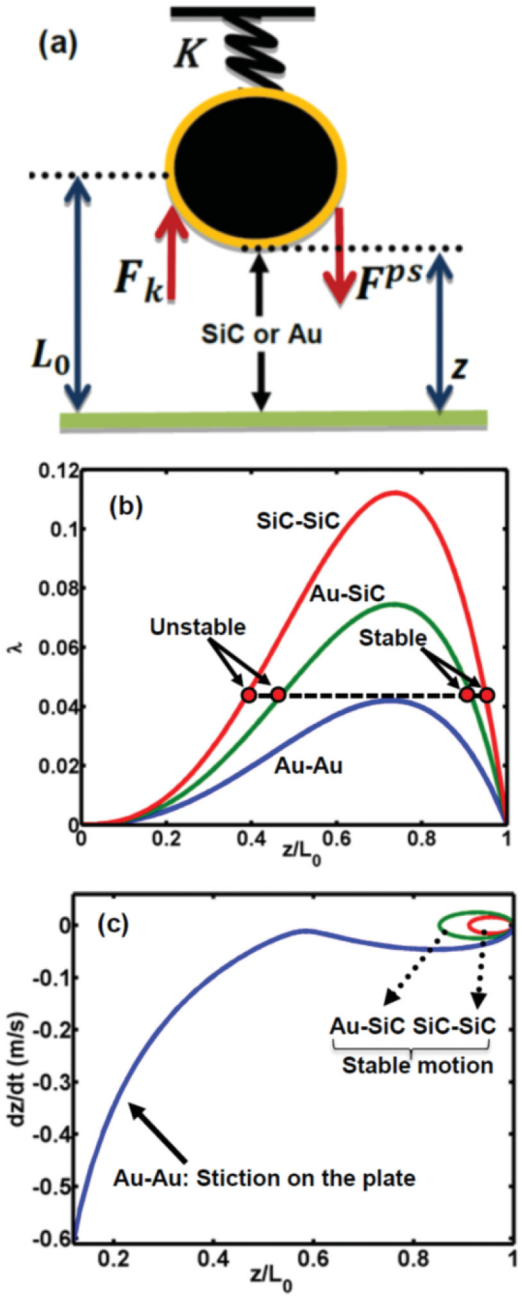

FIG. 6. (Color online) (a) Schematic of an actuated MEM system at initial separation $L_0 = 200$ nm (where the spring is not stretched) with the acting forces. (b) Bifurcation diagrams λ versus z^* for Au-Au and Au/SiC-SiC actuating systems. (c) Phase portrait dz/dt versus z for the Au-Au (open orbit: stiction on the plate) and the Au/SiC-SiC (closed orbit: stable motion) system when $K = 10^{-4}$ N/m.

0 [23,24]. The dependence of λ on the locus of equilibrium points z^* is shown in Fig. 6(b) for all the systems SiC/Au-SiC/Au. The Au-Au is given here for comparison since it is widely used in Casimir force measurements [4–10]. It is evident from Fig. 6(b) that the bifurcation parameter λ is strongly sensitive to changes of the plate optical properties.

Indeed, as Fig. 6(b) shows if the spring constant is strong enough so that $\lambda < \lambda_{\max}$ ($\lambda \sim 1/K$), there are two equilibrium centers. The stationary point closest to L_0 is a stable center around which periodic solutions exist, while the other closer to the plate is an unstable point around which motion will lead to stiction onto the plate due to the stronger Casimir force. The locus of points for $z^* > z^*_{\max}$ corresponds to stable actuation which is apparently strongly increased for SiC. For spring constants K so that $\lambda \geqslant \lambda_{\max}$, for example, for Au, the motion is unstable favoring stiction, while there are still two equilibrium points for the SiC-Au and SiC-SiC systems, one of which is stable. Therefore these results indicate that SiC can enhance the stable "modus operandi" for a MEMS system against stiction instabilities. Although the differences in the bifurcation plots of Fig. 6(b) seem relatively small, investigation of the dynamics via phase portraits (sphere velocity dz/dt versus separation z) can reveal its sensitive dependence on material details. This is in fact illustrated in the phase portrait of Fig. 6(c), where the stronger Casimir force for the Au-Au system leads to stiction, while stable motion (closed orbits) is still feasible for the SiC-SiC and the SiC-Au systems. It is in fact remarkable to see how the size of the stable orbit is reduced if a weaker conductor is used instead of a metal ensuring better protection from stiction instabilities. More details will be given elsewhere of extensive comparison including other nonmetal materials (see, for example, Supplemental Material, Fig. E1 [16]).

VI. CONCLUSIONS

In conclusion, conductive SiC, which is a promising material for systems operating in harsh environments due to its excellent properties (e.g., high hardness, chemical inertness, ability to survive operation at high temperatures, etc.), shows significant far-infrared absorption and sufficient concentration of charge carriers so that one can neglect nonlocal response due to poor conductivity for separations larger than Debye screening length ∼1 nm. As a result of the optical response in the infrared range and beyond to low frequencies, the force approaches slowly the ideal limit upon interaction with metals, while it saturates significantly below the ideal limit if interaction occurs with insulators. Analysis of the van der Waals asymptote at short separations (<10 nm) indicated for SiC-SiC interactions Hamaker constants lower but comparable to those of metallic systems, which is of significance in adhesion-assembly processes. Moreover, the interaction of SiC-Au is comparable with that for Au-Au at separation distances $z <$ 50 nm. Finally, bifurcation and phase portraits analysis of MEMS actuations indicated that SiC can enhance the regime of stable equilibria against stiction instabilities. More in-depth analysis is underway in this direction, in comparison also to less conductive materials than metals, to unravel details during operation in more realistic environments.

ACKNOWLEDGMENTS

We would like to acknowledge support from the Zernike Institute of Advanced Materials, University of Groningen, The Netherlands, and useful discussions with J. Knoester.

[1] A. W. Rodriguez, F. Capasso, and S. G. Johnson, Nat. Photonics **5**, 211 (2011); P. Ball, Nature (London) **447**, 772 (2007).

[2] H. B. G. Casimir, Proc. K. Ned. Akad. Wet. **51**, 793 (1948).

[3] E. M. Lifshitz, Sov. Phys. JETP **2**, 73 (1956); I. E. Dzyaloshinskii, E. M. Lifshitz, and L. P. Pitaevskii, Sov. Phys. Usp. **4**, 153 (1961).

[4] S. K. Lamoreaux, Phys. Rev. Lett. **78**, 5 (1997); Rep. Prog. Phys. **68**, 201 (2005); H. B. Chan, V. A. Aksyuk, R. N. Kleiman, D. J. Bishop, and F. Capasso, Phys. Rev. Lett. **87**, 211801 (2001); Science **291**, 1941 (2001); R. S. Decca, D. López, E. Fischbach, G. L. Klimchitskaya, D. E. Krause, and V. M. Mostepanenko, Ann. Phys. (NY) **318**, 37 (2005); Phys. Rev. D **75**, 077101 (2007).

[5] D. Iannuzzi, M. Lisanti, and F. Capasso, Proc. Natl. Acad. Sci. USA **101**, 4019 (2004).

[6] F. Chen, G. L. Klimchitskaya, V. M. Mostepanenko, and U. Mohideen, Opt. Express **15**, 4823 (2007); G. Torricelli, I. Pirozhenko, S. Thornton, A. Lambrecht, and C. Binns, Europhys. Lett. **93**, 51001 (2011).

[7] S. de Man, K. Heeck, R. J. Wijngaarden, and D. Iannuzzi, Phys. Rev. Lett. **103**, 040402 (2009).

[8] G. Torricelli, P. J. van Zwol, O. Shpak, C. Binns, G. Palasantzas, B. J. Kooi, V. B. Svetovoy, and M. Wuttig, Phys. Rev. A **82**, 010101 (R) (2010).

[9] G. Torricelli, P. J. van Zwol, O. Shpak, G. Palasantzas, V. B. Svetovoy, C. Binns, B. J. Kooi, P. Jost, and M. Wuttig, Adv. Funct. Mater. **22**, 3729 (2012).

[10] C.-C. Chang, A. A. Banishev, G. L. Klimchitskaya, V. M. Mostepanenko, and U. Mohideen, Phys. Rev. Lett. **107**, 090403 (2011).

[11] V. B. Svetovoy, P. J. van Zwol, G. Palasantzas, and J. Th. M. DeHosson, Phys. Rev. B. **77**, 035439 (2008); G. Bimonte, Phys. Rev. A **83**, 042109 (2011).

[12] A. Canaguier-Durand, P. A. Maia Neto, A. Lambrecht, and S. Reynaud, Phys. Rev. A **82**, 012511 (2010).

[13] J. Haisma, N. Hattu, J. T. C. M. Pulles, E. Steding, and J. C. G. Vervest, Appl. Opt. **46**, 6793 (2007); J. Haisma and G. A. C. M. Spierings, Philips J. Res. **49**, 47 (1995); Mater. Sci. Eng., R **37**, 1 (2002).

[14] R. Cheung, in *Silicon Carbide Microelectromechanical Systems for Harsh Environments*, edited by R. Cheung (Imperial College Press, London, 2006), Chap. 1; P. M. Sarro, Sensor Actuator **82**, 210 (2000).

[15] *MEMS Reliability Assurance Guidelines for Space Applications*, edited by B. Stark, Jet Propulsion Laboratory Publications-99-1 (NASA, Pasadena, CA, 1999), http://trs-new.jpl.nasa.gov/dspace/handle/2014/18901.

[16] See Supplemental Material at http://link.aps.org/supplemental/10.1103/PhysRevB.89.195440 for Ellipsometry, AFM topography analysis, optical data analysis, Casimir force calculations, and MEMS actuation analysis for different materials.

[17] P. J. van Zwol, G. Palasantzas, M. van de Schootbrugge, J. Th. M de Hosson, and V. S. J. Craig, Langmuir **24**, 7528 (2008).

[18] W. H. Broer, G. Palasantzas, J. Knoester, and V. B. Svetovoy, Phys. Rev. B **85**, 155410 (2012); Europhys. Lett. **95**, 30001 (2011).

[19] A. Narayanaswamy and G. Chen, Appl. Phys. Lett. **82**, 3544 (2003).

[20] A. Tonck, F. Houze, L. Boyer, J.-L. Loubet, and J.-M. Georges, J. Phys.: Condens. Matter **3**, 5195 (1991).

[21] H.-J. Butt, B. Cappella, and M. Kappl, Surf. Sci. Rep. **59**, 1 (2005); J. N. Israelachvili, *Intermolecular and Surface Forces* (Academic Press, London, 1992); I. Larson, D. Y. C. Chan, C. J. Drummond, and F. Grieser, Langmuir **13**, 2429 (1997); S. Biggs and P. Mulvaney, J. Chem. Phys. **100**, 8501 (1994); V. Kane and P. Mulvaney, Langmuir **14**, 3303 (1998); P. D. Ashby, L. Chen, and C. M. Lieber, J. Am. Chem. Soc. **122**, 9467 (2000).

[22] *Handbook of Optical Constants of Solids*, edited by E. D. Palik (Academic Press, Orlando, FL, 1995).

[23] W. Broer, G. Palasantzas, J. Knoester, and V. B. Svetovoy, Phys. Rev. B **87**, 125413 (2013); M. Sedighi, W. H. Broer, G. Palasantzas, and B. J. Kooi, *ibid.* **88**, 165423 (2013).

[24] R. Esquivel-Sirvent, L. Reyes, and J. Bárcenas, New J. Phys. **8**, 241 (2006); R. Esquivel-Sirvent, M. A. Palomino-Ovando, and G. H. Cocoletzi, Appl. Phys. Lett. **95**, 051909 (2009).

[25] O. Ergincan, G. Palasantzas, and B. J. Kooi, Phys. Rev. B **85**, 205420 (2012); D. M. Karabacak, V. Yakhot, and K. L. Ekinci, Phys. Rev. Lett. **98**, 254505 (2007); K. L. Ekinci, D. M. Karabacak, and V. Yakhot, *ibid.* **101**, 264501 (2008).

[26] R. Garcıa and R. Perez, Surf. Sci. Rep. **47**, 197 (2002); M. Li, H. X. Tang, and M. L. Roukes, Nat. Nanotechnol. **2**, 114 (2007); H. J. Mamin and D. Rugar, Appl. Phys. Lett. **79**, 3358 (2001); D. Rugar, R. Budakian, H. J. Mamin, and B. W. Chui, Nature **430**, 329 (2004).